DOI 10.5012/bkcs.2010.31.9.2547

Preparation and Characterization of Porous and Composite Nanoparticulate Films of CdS at the Air/Water Interface

Guanglei Ji, Kuang-Cai Chen,[†] Yan-Gang Yang,[†] Guoqing Xin,[†] Yong-Ill Lee,[‡] and Hong-Guo Liu[†,*]

College of Resources and Environmental Sciences, University of Jinan, Jinan 250022, China
[†]Key Laboratory for Colloid and Interface Chemistry of Education Ministry, Shandong University, Jinan 250100, China
[*]E-mail: hgliu@sdu.edu.cn
[‡]Department of Chemistry, Changwon National University, Changwon 641-773, Korea
Received January 16, 2010, Accepted July 19, 2010

CdS nano-particulate films were prepared at the air/water interface under Langmuir monolayers of arachidic acid (AA) *via* interfacial reaction between Cd^{2+} ions in the subphase and H_2S molecules in the gaseous phase. The films were made up of fine CdS nanoparticles with hexagonal Wurtzite crystal structure after reaction. It was revealed that the formation of CdS nano-particulate films depends largely on the experimental conditions. When the films were ripened at room temperature or an increased temperature (60 ^{o}C) for one day, numerous holes were appeared due to the dissolution of smaller nanoparticles and the growth of bigger nanoparticles with an improved crystallinity. When the films were ripened further, CdS rodlike nanoparticles with cubic zinc blende crystal structure appeared due to the re-nucleation and growth of CdS nanoparticles at the stacking faults and defect structures of the hexagonal CdS grains. These structures were characterized by transmission electron microscopy (TEM), high-resolution TEM (HRTEM), and X-ray diffraction (XRD). These results declare that CdS semiconductor nanoparticles formed at the air/water interface change their morphologies and crystal structures during the ripening process due to dissolution and recrystallization of the particles.

Key Words: CdS, Porous Film, Nanorod, Langmuir monolayer, Ostwald ripening

Introduction

As a wide band-gap semiconductor, cadmium sulfide (CdS) has been widely used in the fields of solar cells for photoelectric conversion, light-emitting diodes for flat-panel displays, sensors, and photocatalysis. Quantum dots[1] and anisotropic nanoparticles including CdS nanorods[2] and nanowires[3] have been extensively studied, because the properties of nanostructures depend on their sizes and shapes, and various preparation methods. At the same time, nano-particulate CdS thin films have attracted much attention. Those films have been prepared by various approaches, such as vacuum evaporation,[4] sputtering,[5] molecular beam epitaxy,[6] chemical vapor deposition,[7] spray pyrolysis,[8] chemical bath deposition,[9] electrochemical co-deposition[10] and annealing Cd^{2+}-dithiol self-assembled films.[11]

The chemical reactions occurred at the air/water interface have been widely utilized to synthesize inorganic nanoparticles and nano-particulate films. In fact, CdS nanoparticles and nanoparticulate films have been prepared at the air/water interface *via* interfacial reactions between Cd^{2+} in the subphase and H_2S in the gaseous phase. The nanoparticles with anisotropic shapes usually formed at the air/water interface by forming them under a restriced microenvironment. On the other hand, the Langmuir monolayers of amphiphilic molecules formed at the air/water interface not only enrich the metal ions from the subphase, but also direct the nucleation and growth of the nanoparticles with special crystal faces. Therefore, it results in the formation of highly-oriented nanoparticles and nanoparticle arrays. Yang *et al.*[12] synthesized oriented CdS nanorods with hexagonal Wurtzite structure at the air/water interface templated by arachidic acid monolayers. While Pan *et al.*[13] prepared the oriented rod-like and dot-like CdS nanoparticles with cubic zinc blende structure at the air/water interface templated by stearic acid monolayers. They demonstrated that lattice matching between the two-dimensional arrays of the head groups of fatty acids and the special faces of CdS crystal should be responsible for the formation of the oriented nanoparticles. Berman *et al.*[14] synthesized one-dimensional chains of CdS nanoparticles with cubic zinc blende structure at the air/water interface under Langmuir monolayers of a linear polymer. In this case, the monolayer of the linear polymer acted not only as a template for the nucleation of special facets via lattice matching, but also as a linear template to organize the formed nanoparticles. Recently, we prepared the hexagonal platelike aggregates of CdS with hexagonal Wurtzite structure under Langmuir monolayers of amphiphilic porphyrin derivative molecules.[15] It suggested that the hexagonal platelike aggregates were formed by the self-organization and oriented attachment of CdS nanoparticles at the interface. In addition, nano-particulate CdS films were prepared successfully at the air/water interface *via* interfacial chemical reactions. These studies deal with the formation process of the nano-particulate films and the influences of experimental conditions such as pH values and concentrations of the precursors, on the characteristics of the films and limited thickness of the films.[16-22]

The air/water interface has also been utilized to synthesize and fabricate nanostructures *via* the self-organization of inorganic species and surfactants in the liquid phase during the reaction process. Mesoporous silica thin films[23] and networks of platinum nanoparticles[24] were prepared at the air/water interfaces. We also found that the nanoparticles formed at the air/water interface would dissolve, re-crystallize, re-organize and be

etched selectively to form new nanostructures. In our previous studies, the hexagonal and round CdS nanorings[15] and single-crystalline PbS nanorings[25] have been prepared by using this strategy.

In this paper, we describe the formation of porous and composite CdS nano-particulate films during the ripening process after the interfacial reaction. We clearly observed that the preformed CdS nanoparticles with hexagonal Wurtzite structure transformed to nanorods with cubic zinc blende structure after recrystallization, and composite nano-particulate films with these two kinds of crystal structures formed. These composite nano-particulate films are of great importance on their photocatalytic properties and applications. For example, Silva *et al.*[26] used a hybrid system composed of nanoparticulate CdS with cubic zinc blende structure and bulk phase hexagonal CdS interlinked with Pt deposits as a photocatalyst to produce H_2 from water under visible light irradiation. They found that the hybrid system has higher photocatalytic activity than other systems, such as the composites of CdS with pure crystal structure with Pt, and the CdS with hexagonal or cubic structure only. In addition, the phase transition in CdS thin films has been received much attention in recent years.[27-29]

Experimental Section

Chemicals. Arachidic acid (> 99.0%) and cadmium chloride (> 99.0%) were purchased from Shanghai Chemical Co. Chloroform, sodium sulfide ($Na_2S·9H_2O$), and sulfuric acid are analytical reagents. Highly purified water was used with a resistivity greater than 18 MΩ·cm.

Preparation of the thin film, porous film, and nanorods of CdS. Aqueous $CdCl_2$ solutions with the concentrations of 1×10^{-4}, 1×10^{-3} and 1×10^{-2} mol L^{-1} were prepared as subphase. The chloroform solution of arachidic acid with the concentration of 0.1 mg mL^{-1} was used as spreading solution. Four beakers with an inner diameter of 5.7 cm that contained 10.0 mL of the subphase solution were placed in a container with a volume of 5 L, and then 66 μL of the AA chloroform solution was spread on the subphase surface in each beaker by using a microsyringe to form a condensed monolayer. After evaporation of chloroform for 15 min, H_2S gas was produced by the reaction of H_2SO_4 with Na_2S in another beaker in the container, and then the container was sealed immediately. A fresh Na_2S aqueous solution was prepared before use by dissolving 0.1070 g $Na_2S·9H_2O$ in 10 mL H_2O. The total amount of H_2S was controlled to be 4.0 mL by using 4.0 mL Na_2S aqueous solution and excess 1:1 H_2SO_4. The reaction was carried out at room temperature for 1 h.

After reaction, the beakers were placed in another clean sealed container which was placed in an oven. The temperatures for ripening were controlled to be 20 °C or 60 °C for different periods, such as 1, 3 and 5 days.

Characterization. The production was transferred onto Formvar-covered or carbon-coated copper grids and hydrophobic quartz slides by the Langmuir-Schäfer method for transmission electron microscopy (TEM, JEM-100CXII), high-resolution transmission electron microscopy (HRTEM, GEOL-2010), UV-vis spectroscopy (HP 8453E) and X-ray diffraction (XRD, Rigaku D/Max 2200PC) investigations, respectively.

Results and Discussion

Figure 1 shows the TEM micrographs of CdS nano-particulate films produced at the air/water interafce. As can be seen in the image, a compact film was composed of nanoparticles with different sizes. The TEM micrographs of the porous films after ripening under different conditions were illustrated in Figure 2. When the concentration of the subphase was 1×10^{-4} mol L^{-1}, a lot of round holes with the diameter of 100 ~ 200 nm appeared after ripening for 1 day at room temperature. The holes have thicker walls. These holes should be considered as ringlike nanostructures in a sense. As the ripening temperature rose to 60 °C, the number of the holes increased, as shown in Figure 2b. When the concentration of subphase increased to 1×10^{-3} mol L^{-1}, bigger holes with the diameter of about 300 nm appeared after ripening for 2 days at 60 °C, and a porous film with big holes emerged after 3 days, as shown in Figure 2d. Figure 2e displays the corresponding SAED pattern which gives clear discontinued diffraction rings that can be indexed to hexagonal Wurtzite crystal structure of CdS. There are elongated diffrac-

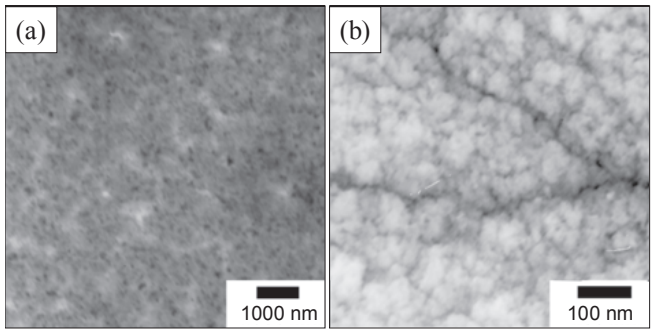

Figure 1. TEM micrographs of CdS nanoparticulate films formed at the air/water interface.

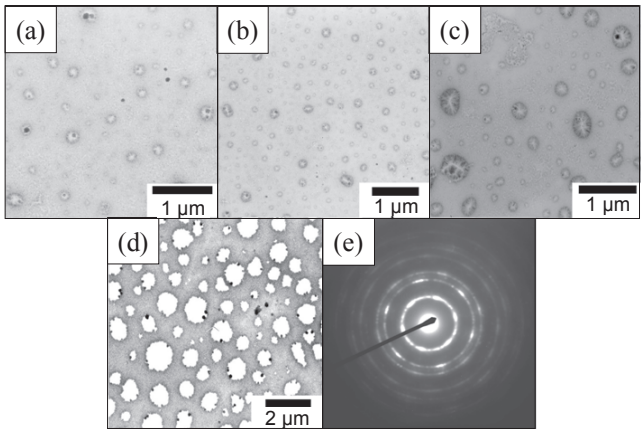

Figure 2. TEM micrographs of CdS ring-like nanostructures formed at the air/water interface after ripening under different conditions. The subphase concentrations, ripening temperatures, and ripening times are 1×10^{-4} mol L^{-1}, room temperature, 1 day (a); 1×10^{-4} mol L^{-1}, 60 °C, 1 day (b); 1×10^{-3} mol L^{-1}, 60 °C, 2 days (c); and 1×10^{-3} mol L^{-1}, 60 °C, 3 days (d), respectively. The SAED pattern (e) corresponds to (c).

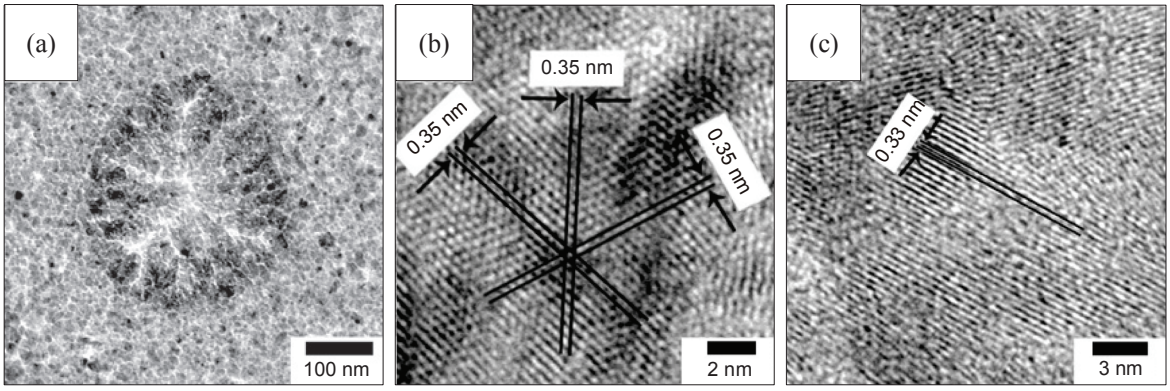

Figure 3. HR-TEM images of one hole on the CdS porous film.

tion spots with six-fold symmetry, indicating that most of the formed CdS nanoparticles have similar orientation in the film.

Figure 3 presents the HR-TEM images of a hole in the porous film. In Figure 3a we can see that the thin film is made up of a large quantity of small nanocrystals. Two-dimensional lattice image (Fig. 3b) gives apparent arrays with six-fold symmetry. The interplanar spacings were measured to be 0.35 nm, which is in accordance to 0.358 nm, the $d_{(100)}$ of the Wurtzite CdS crystal (PDF No. 650-3414), indicating that most of the CdS nanocrystals have the orientation with their (001) face parallel to the air/water interface. This coincides with the SAED pattern in Figure 2e. Figure 3c gives the lattice image with the interplanar spacing of 0.33 nm, closing to 0.337 nm, the $d_{(002)}$ of the Wurtzite CdS crystal. This implies that some nanocrystals have the orientation with their (100) face parallel to the interface. It has been observed that the particles at the hole edge are larger than those in the film (Figure 3a).

The formation of the holes and the porous film should be attributed to Ostwald ripening of the nano-particulate films. As can be seen in Figure 1, the films are composed of numerous nanocrystals with various sizes. It is well known that the solubility of the particles depends on their size according to the following equation

$$\ln(X_r/X) = (2\gamma M)/(RTr\rho)$$

Where X_r and X represent the solubilities of a small particle with the radius of r and the corresponding bulk phase, respectively; and γ, M, and ρ represent the interfacial tension at the solid-liquid interface, the mole mass and density of the solid, respectively. It can be deduced that smaller nanoparticals have higher solubility. They dissolved gradually and then led to the formation of smaller holes. After a hole formed, the contact area of the hole inner edge in subphase solution increased. The dissolution process was then accelerated, leading to the formation of bigger holes. When the concentration of CdS in the solution increased up to a critical value, the species in the solution was re-crystallized gradually, resulting in the formation of thicker walls, as shown in Figures 2a-c.

When the subphase concentration increased to 1×10^{-2} mol L^{-1}, rodlike nanocrystals appeared in the films besides the holes after ripening for five days at 60 °C. Figure 4 shows the

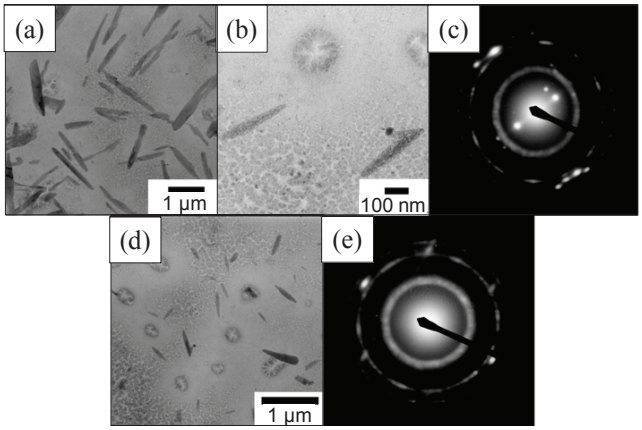

Figure 4. TEM micrographs of CdS rod-like nanostructures formed at the air/water interface after ripening at 60 °C for 5 days. The subphase concentration is 1×10^{-2} mol L^{-1}. The SAED pattern (c) corresponds to (b); The SAED pattern (e) corresponds to (d).

TEM micrographs of the formed nanorods and the corresponding ED patterns. It is evident that the nanorods were produced under the nano-particulate films. The nanorods shown in Figure 4a have the length of *ca.* 1 μm. It was also observed that the rodlike nanostructure is composed of parallel aligned short nanorods through the high-magnification image shown in Figure 4b. Figure 4d exhibits another kind of nanorods which have the length of several hundreds of nanometers. The corresponding ED patterns give discontinued diffraction rings and spots (Figures 4c and 4e).

The rodlike nanostructures were characterized by HRTEM. Figure 5 represents the HRTEM image of the rodlike nanostructures shown in Figure 4a. The length of the nanostructure reaches to several micrometers. It was revealed that they are composed of parallel aligned short rods (Figure 5b). Square two-dimensional lattice images can also be seen from Figure 5c. The interplanar distance was measured to be 0.27 nm, closing to 0.292 nm, the $d_{(200)}$ of cubic zinc blende CdS (PDF No. 65-2887), indicating that the formed nanorods have cubic crystal structure and the nucleation face is (001) plane, with the growth direction of [100]. It can be also seen that some black and white strips formed, which have the same direction as the short rods. So the ED pattern shown in Figure 4c can be considered as the

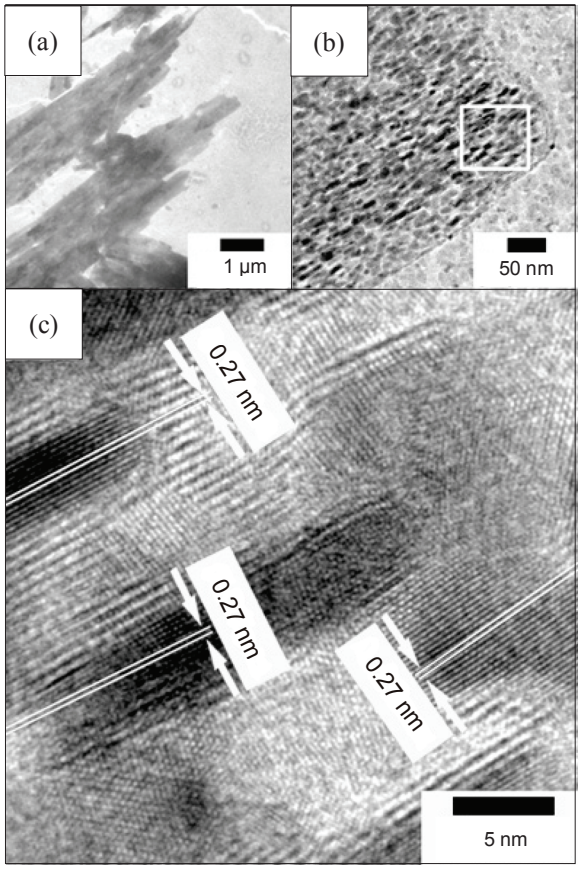

Figure 5. HR-TEM images of rod-like CdS nanostructures corresponding to Figure 4(a).

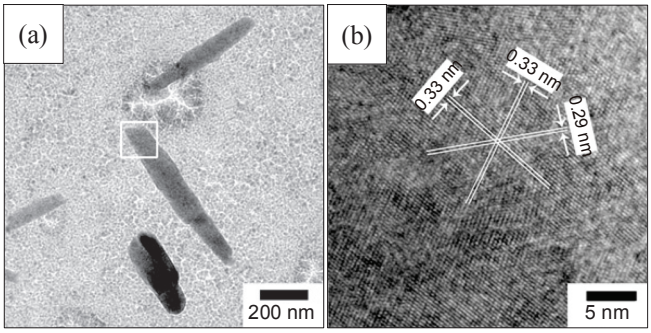

Figure 6. HR-TEM images of rod-like CdS nanostructures corresponding to Figure 4(d).

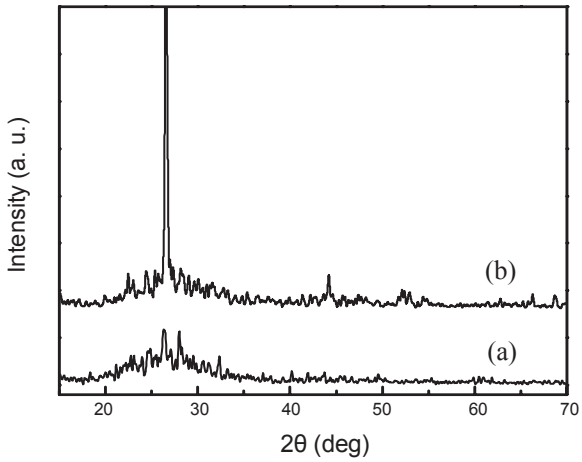

Figure 7. XRD spectra of CdS films after ripening for 1 day (a) and 5 days at 60 °C (b). The subphase concentration is 1×10^{-2} mol L^{-1}

superimposition of the diffraction pattern of hexagonal Wurtzite CdS of the background films and that of the cubic zinc blende CdS of the nanorods. The two bright spots near the center should correspond to the strip structures.

Figure 6 shows the HRTEM image of the nanorods corresponding to Figure 4d. Two-dimensional lattice image appeared. The interplanar distances were measured to be 0.33, 0.33 and 0.29 nm, closing to 0.337 and 0.292 nm, the $d_{(111)}$ and $d_{(200)}$ of the cubic zinc blende CdS (PDF No. 65-2887), respectively, indicating that the formed nanorods have cubic crystal structure, and the nucleation face is (110) plane. Similarly, the ED pattern shown in Figure 4e should be the superposition of hexagonal and cubic CdS.

The formation of the nanorods with cubic zinc blende crystal structure was confirmed further by XRD spectra shown in Figure 7. Three main peaks with 2θ angles of 25.19°, 26.13° and 28.23° appear in the spectrum of the sample ripened for 1 day, while at least five peaks appear at 25.23°, 26.29°, 28.25°, 44.23° and 52.31° after 5-day ripening. According to the PDF cards, the diffraction peaks of (101), (100) and (002) planes of hexagonal CdS appear at 25.13°, 26.19° and 28.17°, and the diffraction peaks of (111), (220) and (311) planes of cubic CdS appear at 26.19°, 44.15° and 52.15°, respectively. So the peaks in curve (a) should be indexed to those of hexagonal CdS, while the peaks in (b) should be indexed to both hexagonal and cubic CdS. This confirms further that hexagonal CdS formed after reaction and short time ripening, whereas cubic CdS appeared after long time ripening. It should be pointed out that the intensity of peak at 26.29° in curve b is obviously higher than the intensities of other peaks. This may be attributed to the improvement of the crystallinity, the superposition of the (111) peak of cubic CdS and the (100) peak of hexagonal CdS and the preferential orientation of the particles.

During the ripening process, small particles dissolved and water evaporated gradually, leading to the increase of the concentration of CdS in the subphase. When the concentration reached to a critical value, CdS particles commence to re-crystallize from the subphase, resulting in the nucleation and growth of CdS particles that attached on the CdS films at the air/water interface. It was found that two kinds of nanorods of CdS with cubic zinc blende structure were formed during the ripening process, as shown in Figures 5 and 6, respectively. These two kinds of nanorods should have different formation mechanisms. The nanorods in Figure 5 have the nucleation face of (001) plane. A large numbers of stacking faults or defects such as the strips which are parallel to the nanorods of CdS with cubic structure were observed, as shown in Figure 5c. It may possible that the strip structure induced the formation of the aligned short rods in parallel. On the other hand, the nanorods shown in Figure 6 were generated under the homogeneous

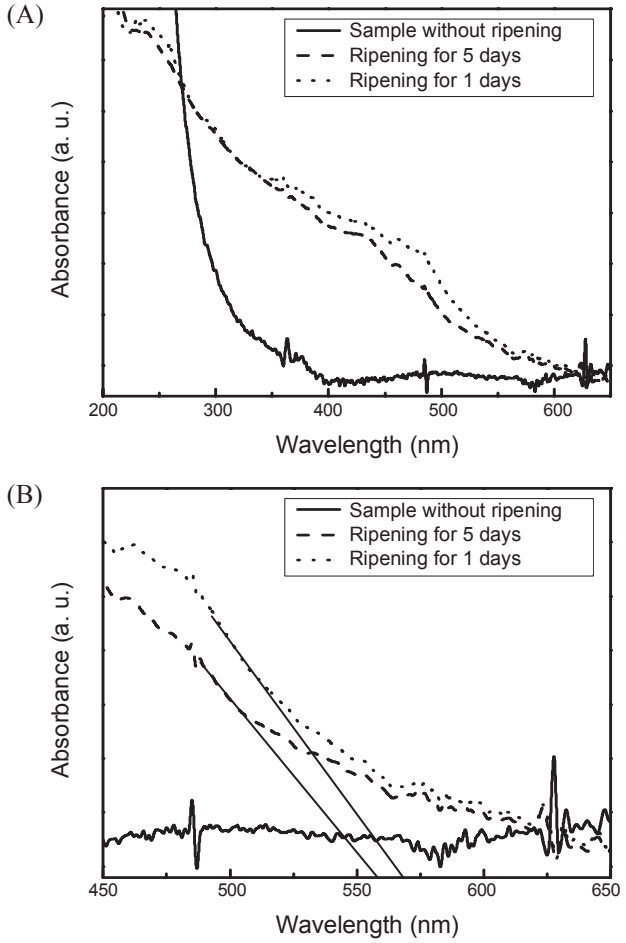

Figure 8. UV-vis spectra of the formed films (A) and the enlarged ones (B).

CdS film, which have the nucleation face of (110) plane. The homogeneous CdS film should be composed of hexagonal Wurtzite CdS nanoparticles with their (001) or (100) faces in parallel to the interface, as indicated in Figure 3. The measured $d_{(111)}$ of the cubic CdS is 0.33 nm, closing to 0.33 or 0.35 nm, the measured $d_{(002)}$ or $d_{(100)}$ of the hexagonal CdS in Figure 3. It is possible that the lattice matching between the (110) face of the cubic CdS and (100) or (001) face of the hexagonal CdS leads to the formation of the nanorods of CdS with cubic structure shown in Figure 6.

The optical properties of the CdS samples were investigated by using UV-vis spectroscopy. As can be seen in Figure 8, the sample without ripening gives a sharp peak at 362 nm, indicating that the formed CdS nano-particulate film are composed of fine clusters.[30] The sample ripened for 1 day shows a red-shifted edge absorption at ~570 nm, indicating the growth of the bigger particles with hexagonal crystal structure during the ripening process. However, the sample ripened for 5 days shows a blue-shifted edge absorption at ~560 nm compared with that of the sample ripened for 1 day. This means the appearance of the particles with cubic structure.[26] This result further confirms the formation of the nanorods with cubic crystal structure under long time ripening, consistent with the TEM, HRTEM and XRD investigations.

Conclusions

Nano-particulate thin films composed of CdS clusters with hexagonal crystal structure were prepared successfully at the air/water interface *via* interfacial reaction under arachidic acid Langmuir monolayers. After ripening at room temperature or higher temperature, some clusters dissolved and other clusters grew to form porous thin films through an Ostwald ripening process. After ripening further, rod-like nanoparticles with cubic crystal structure were formed, leading to the formation of composite films. It is noteworthy that our development is an interesting way to get such composite nanostructures efficiently.

Acknowledgments. The authors thank the financial support of National Natural Science Foundation of China (Grant No. 20873078) and Priority Research Centers Program through the National Research Foundation of Korea (NRF) funded by the Ministry of Education, Science and Technology (NRF 2009-0094066).

References

1. Torimoto, T.; Kontani, H.; Shibutani, Y.; Kuwabata, S.; Sakata, T.; Mori, H.; Yoneyama, H. *J. Phys. Chem. B* **2001**, *105*, 6838.
2. Liang, H.; Angelini, T. E.; Braun, P. V.; Wong, G. C. L. *J. Am. Chem. Soc.* **2004**, *126*, 14157.
3. Liu, X.-L.; Zhu, Y.-J. *Mater. Lett.* **2009**, *63*, 1085.
4. Senthil, K.; Mangalaraj, D.; Narayandass, S. K.; Kesavamoorthy, R.; Reddy, G. L. N. *Nucl. Instr. and Meth. in Phys. Res. B* **2001**, *173*, 475.
5. Ximello-Quiebras, J. N.; Mejía-García, C.; Caballero-Rosas, A.; Hernandez-Contreras, H.; Contreras-Puente, G.; Vidal, J.; Pascher, H. *Thin Solid Films* **2003**, *431-432*, 223.
6. Choi, J. W.; Bhupathiraju, A.; Hasan, M.-A.; Lannon, J. M. *J. Cryst. Growth* **2003**, *255*, 1.
7. Uda, H.; Yonezawa, H.; Ohtsubo, Y.; Kosaka, M.; Sonomura, H. *Solar Energy Materials Solar Cells* **2003**, *75*, 219.
8. Baykul, M.C.; Balcioglu, A. *Microelectronic Engineering* **2000**, *51-52*, 703.
9. Hiie, J.; Dedova, T.; Valdna, V.; Muska, K. *Thin Solid Films* **2006**, *511-512*, 443
10. Torimoto, T.; Nagakubo, S.; Nishizawa, M.; Yoneyama, H. *Langmuir* **1998**, *14*, 7077.
11. Zhang, Y.; Mu, J. *Colloids Surf. A* **2005**, *262*, 238.
12. Yang, J.; Meldrum, F. C.; Fendler, J. H. *J. Phys. Chem.* **1995**, *99*, 5500.
13. Pan, Z. Y.; Liu, X. J.; Zhang, S. Y.; Shen, G. J.; Zhang, L. G.; Lu, Z. H.; Liu, J. Z. *J. Phys. Chem. B* **1997**, *101*, 9703.
14. Berman, A.; Charych, D. *Adv. Mater.* **1999**, *11*, 296.
15. Xiao, F.; Liu, H.-G.; Wang, C.-W.; Lee, Y.-I.; Xue, Q.; Chen, X.; Hao, J.; Jiang, J. *Nanotechnology* **2007**, *18*, 435603.
16. Zhao, X. K.; McCormick, L.; Fendler, J. H. *Chem. Mater.* **1991**, *3*, 922.
17. Yi, K. C.; Fendler, J. H. *Langmuir* **1990**, *6*, 1519.
18. Yuan, Y.; Cabasso, I.; Fendler, J. H. *Chem. Mater.* **1990**, *2*, 226.
19. Zhao, X. K.; Fendler, J. H. *Chem. Mater.* **1991**, *3*, 168.
20. Zhao, X. K.; Xu, S.; Fendler, J. H. *Langmuir* **1991**, *7*, 520.
21. Zhao, X. K.; Fendler, J. H. *J. Phys. Chem.* **1991**, *95*, 3716.
22. Yu, W. L.; Huang, W.; Zhu, B. Y.; Zhao, G. X. *Mater. Lett.* **1997**, *33*, 221.
23. Yang, H.; Coombs, N.; Sokolov, I.; Ozin, G. A. *Nature* **1996**,

381, 589.
24. Chen, H.; Dong, S. *Langmuir* **2007**, *23*, 12503.
25. Xin, G.-Q.; Ding, H.-P.; Yang, Y.-G.; Shen, S.-L.; Xiong, Z.-C.; Chen, X.; Hao, J.; Liu, H.-G. *Cryst. Growth Des.* **2009**, *9*, 2008.
26. Silva, L. A.; Ryu, S. Y.; Choi, J.; Choi, W.; Hoffmann, M. R. *J. Phys. Chem. C* **2008**, *112*, 12069.
27. Lincot, D.; Mokili, B.; Froment, M.; Cortes, R.; Bernard, M. C.; Witz, C.; Lafait, J. *J. Phys. Chem. B* **1997**, *101*, 2174.
28. Zelaya-Angel, O.; Hernandez, L.; de Melo, O.; Alvarado-Gil, J. J.; Lozada-Morales, R.; Falcony, C.; Vargas, H.; Ramirez-Bon, R. *Vaccum* **1995**, *46*, 1083.
29. Sisman, I.; Alanyalioglu, M.; Demir, U. *J. Phys. Chem. C* **2007**, *111*, 2670.
30. Li, M.; Ouyang, J.; Ratcliffe, C. I.; Pietri, L.; Wu, X.; Leek, D. M.; Moudrakovski, I.; Lin, Q.; Yang, B.; Yu, K. *ACS Nano* **2009**, *3*, 3832.